Noise-induced macroscopic oscillations in a network of synaptically coupled quadratic integrate-and-fire neurons

Irmantas Ratas and Kestutis Pyragas
Center for Physical Sciences and Technology, LT-10257 Vilnius, Lithuania

(Received 8 May 2019; published 21 November 2019)

We consider the effect of small independent local noise on a network of quadratic integrate-and-fire neurons, globally coupled via synaptic pulses of finite width. The Fokker-Planck equation for a network of infinite size is reduced to a low-dimensional system of ordinary differential equations using the recently proposed perturbation theory based on circular cumulants. A bifurcation analysis of the reduced equations is performed, and areas in the parameter space, where the noise causes macroscopic oscillations of the network, are determined. The validity of the reduced equations is verified by comparing their solutions with "exact" solutions of the Fokker-Planck equation, as well as with the results of direct simulation of stochastic microscopic dynamics of a finite-size network.

DOI: 10.1103/PhysRevE.100.052211

I. INTRODUCTION

Understanding the macroscopic behavior of complex systems consisting of large numbers of interacting oscillators or excitable elements is of great interest because such systems occur in a wide variety of significant applications [1–3]. Synchronization between the elements constituting such systems may lead to the occurrence of oscillating macroscopic fields. Such a phenomenon is well explained by the Kuramoto paradigmatic model [1,4], which describes a system of globally coupled phase oscillators with distributed natural frequencies. Ott and Antonsen [5] analyzed this model in the infinite-size (thermodynamic) limit and found that it displays low-dimensional dynamics that can be described by a macroscopic order parameter governed by a simple nonlinear differential equation. The dimensionality reduction approach developed in Ref. [5] is known as the Ott-Antonsen (OA) *Ansatz*. It has been successfully applied in a number of subsequent publications for various networks of phase oscillators [6–11] (see also Ref. [12] for a recent review).

Synchronization effects are of particular interest in neuroscience. In the brain, oscillations are a prominent feature of neuronal activity and the synchronization of oscillations is a mechanism for neural communication, which endows individual brain areas with the ability to perform specific tasks [13]. Abnormal synchronization can cause neurological diseases like Parkinson's disease [14–17]. Simple models of neural networks help us to understand the synchronization mechanism in neural systems. One such model is a heterogeneous network of globally coupled quadratic integrate-and-fire (QIF) neurons. The QIF neuron is the canonical model for the class I neurons near the spiking threshold [18]. The QIF neuron model can be transformed into a theta neuron model using a simple variable transformation. The network consisting of theta neurons admits an analytical treatment via the OA *Ansatz* [19–22]. Thus, the QIF neural network, after a suitable transformation, can also be treated with the OA *Ansatz*. Alternatively, the QIF neural network model can be directly reduced to a low-dimensional system using the Lorentzian *Ansatz* (LA) [23]. The order parameters of the OA and LA *Ansätzes* are related with each other by a simple conformal mapping. The LA *Ansatz* has been successfully applied in recent publications to analyze the occurrence of macroscopic oscillations in networks of QIF neurons with a realistic synaptic coupling [24], in the presence of a delay in couplings [25,26], in an inhibitory network with finite synaptic time [27], in the case of heterogeneous coupling [28], as well as in two interacting populations [29].

The AO and LA *Ansätzes* are applicable only for noiseless networks. Although noise is an important ingredient in neural systems [30], the low-dimensional theory for QIF neural networks in the presence of noise is still lacking. The aim of this work is to fill the gap. In this paper, we consider a network of globally coupled QIF neurons subjected to independent local noise. The interaction between neurons is provided by synaptic pulses of a finite width [24]. We apply the newly developed method of circular cumulants [31–33], and we derive a low-dimensional system of ordinary differential equations that describes the macroscopic behavior of a network in the thermodynamic limit. The obtained low-dimensional model allows us to perform a bifurcation analysis of the system and determine the regions in the parameter space where noise induces macroscopic oscillations.

The effect of noise on nonlinear dynamical systems has been a topic of great interest in recent decades [34]. The greatest influence of noise occurs near the bifurcation points. An example is the coherence resonance [35] observed in a noise-driven excitable system near the excitability threshold. In a network of interacting excitable elements, noise can induce global synchronous oscillations. Such a collective effect was first demonstrated numerically for an ensemble of globally coupled active rotators [36]. Later this model and its various modifications were comprehensively studied by different authors [37–40]. Noise-induced coherent oscillations

were also considered in networks of excitable integrate-and -fire neurons [41,42] as well as FitzHugh-Nagumo neurons [43–48] (see Ref. [49] for a review). Most of the previous studies considered only the diffusive coupling between excitable elements, while here we analyze the QIF neurons interacting via synaptic pulses. The low-dimensional model derived here can be considered as an alternative to the phenomenological neural mass models that are used to simulate the coarse-grained activity of large populations of neurons [50].

The paper is organized as follows. In Sec. II, we describe the stochastic QIF neural network model and transform it into a network of theta neurons. Then, in the thermodynamic limit, we reduce the corresponding Fokker-Planck equation to a low-dimensional system of equations for two circular cumulants. Section III is devoted to bifurcation analysis of the reduced equations and a comparison of their solutions with "exact" solutions of the Fokker-Planck equation, as well as with the results of direct simulation of a microscopic network model. Finally, in Sec. IV we discuss our results.

II. LOW-DIMENSIONAL REDUCTION OF THE STOCHASTIC QIF NEURAL NETWORK MODEL

A. Microscopic model

We consider a network of N all-to-all coupled quadratic integrate-and-fire neurons subjected to local Gaussian noise. The microscopic state of the network is defined by the set of neurons' membrane potentials $\{V_j\}_{j=1,\dots,N}$, which satisfy the following equations:

$$\dot{V}_j = V_j^2 + \eta_j + S + \sigma\xi_j(t). \tag{1}$$

Here the constants η_j specify the behavior of individual neurons, S stands for the synaptic current, and the last term $\sigma\xi_j(t)$ represents independent white Gaussian noises with $\langle\xi_j(t)\rangle = 0$ and $\langle\xi_i(t)\xi_j(t')\rangle = \delta_{ij}\delta(t-t')$, where σ governs the amplitude of noise, δ_{ij} is the Kronecker delta, and $\delta(t-t')$ is the Dirac delta function. Each moment the membrane potential V_j reaches the peak value V_{peak}, its voltage is reset to the value V_{reset}. To simplify future analysis, we set $V_{\text{peak}} = -V_{\text{reset}} \to \infty$. We also assume that synaptic dynamics is fast and the synaptic current can be written as [24]

$$S \equiv S(t) = J\frac{V_{\text{th}}}{N}\sum_{i=1}^{N} H[V_i(t) - V_{\text{th}}]. \tag{2}$$

Here J represents the coupling strength, $H(\cdot)$ is the Heaviside step function, and V_{th} is a threshold potential. The positive and negative signs of J correspond to the excitatory and inhibitory interactions, respectively. At the moment t, only those neurons whose membrane potential $V_i(t)$ exceeds the threshold value V_{th} contribute to the synaptic current. In fact, the parameter V_{th} determines the width and height of the synaptic pulses. When the ith neuron spikes, the therm $V_{\text{th}}H[V_i(t) - V_{\text{th}}]$ generates rectangular pulses of height V_{th}. The width of the pulses for large V_{th} can be approximated as $1/V_{\text{th}}$ [24]. When $V_{\text{th}} \to \infty$, the pulses turn into Dirac δ spikes of zero width.

The noiseless ($\sigma = 0$) and isolated ($S = 0$) QIF neuron is the canonical model for the class I neurons near the spiking threshold. The spiking instability in such neurons appears through a saddle-node bifurcation on an invariant curve (SNIC), in which a pair of fixed points on a closed curve coalesce to disappear, converting the curve to a periodic orbit. A remarkable feature of a system following this scenario is that it exhibits excitability before the bifurcation. For the QIF neuron, this scenario is provided by the bifurcation parameter η_j. For $\eta_j < 0$, the neuron is in an excitable regime, and for $\eta_j > 0$ it is in the spiking regime. Generally, we suppose that the values of the parameters η_j are distributed according to some defined density function $g(\eta)$.

Analytical processing and numerical simulation of the model are more convenient after changing variables

$$V_j = \tan(\theta_j/2) \tag{3}$$

that turn QIF neurons into theta neurons. Such a transformation of variables allows us to avoid the problem associated with jumps of infinite size (from $+\infty$ to $-\infty$) of the membrane potential V_j of the QIF neuron at the moments of firing. The phase θ_j of a theta neuron simply crosses the value of $\theta_j = \pi$ at these moments. For theta neurons, Eqs. (1) transform to

$$\dot{\theta}_j = 1 - \cos\theta_j + (1+\cos\theta_j)[\eta_j + S + \sigma\xi_j(t)]. \tag{4}$$

In Eqs. (1) noise is additive, while here it is multiplicative. Equations (4) should be interpreted in the sense of Stratonovich [51].

B. Thermodynamic limit $N \to \infty$

In the limit of an infinite number of neurons, the state of the system can be described by the Fokker-Planck equation

$$\frac{\partial\rho}{\partial t} = -\frac{\partial}{\partial\theta}\left\{\left[f + \frac{h}{2}\frac{\partial h}{\partial\theta}\right]\rho\right\} + \frac{1}{2}\frac{\partial^2}{\partial\theta^2}(h^2\rho). \tag{5}$$

Here $\rho = \rho(\theta|\eta, t)$ is the probability density function (PDF) that defines the density of theta neurons with phase θ and parameter η at time t. The functions $f = f(\theta)$ and $h = h(\theta)$ are as follows:

$$f = 1 - \cos(\theta) + [1+\cos(\theta)](\eta + S), \tag{6a}$$

$$h = \sigma[1+\cos(\theta)]. \tag{6b}$$

In the thermodynamic limit, the sum in Eq. (2) should be replaced by the integral

$$S = JV_{\text{th}}\int_{-\infty}^{+\infty} g(\eta)\int_{-\pi}^{\pi}\rho(\theta|\eta,t)H\left[\tan\left(\frac{\theta}{2}\right) - V_{\text{th}}\right]d\theta\, d\eta. \tag{7}$$

Following the Ott-Antonsen theory [5], we expand the PDF in Fourier series

$$\rho(\theta|\eta,t) = \frac{1}{2\pi}\left\{a_0 + \left[\sum_{j=1}^{\infty} a_j(\eta,t)e^{-ij\theta} + \text{c.c.}\right]\right\} \tag{8}$$

with $a_0 = 1$ due to the normalization condition, and we rewrite Eq. (5) as an infinite system for the complex

amplitudes of the Fourier modes,

$$\dot{a}_j = ij(S+\eta+1)a_j + \frac{i}{2}j(S+\eta-1)(a_{j+1}+a_{j-1}) + \frac{\sigma^2 j}{4}[(1-2j)a_{j-1} - (1+2j)a_{j+1} - 3ja_j] + \frac{\sigma^2 j}{8}[(1-j)a_{j-2} - (1+j)a_{j+2}], \quad j \geqslant 1. \tag{9}$$

The amplitudes $a_j = \int_{-\pi}^{\pi} \rho(\theta|\eta,t)e^{ij\theta}d\theta$ are the local order parameters at a given η. The global Kuramoto-Daido order parameters are obtained by the averaging of these amplitudes over the distribution of the parameter η:

$$Z_j(t) = \int_{-\infty}^{+\infty} g(\eta)a_j(\eta,t)d\eta. \tag{10}$$

Below we consider the Lorentzian distribution

$$g(\eta) = \frac{1}{\pi}\frac{\Delta}{(\eta-\bar{\eta})^2+\Delta^2}, \tag{11}$$

where Δ and $\bar{\eta}$ are the width and the center of the distribution, respectively. We adopt Ott-Antonsen's assumption [5] on the analyticity of $a_j(\eta,t)$ as a function of complex η in the upper half-plane. Then by using the residues theorem, we obtain the following expression for the global Kuramoto-Daido order parameters:

$$Z_j(t) = a_j(\bar{\eta}+i\Delta,t), \tag{12}$$

and we derive for them an infinite system of equations,

$$\dot{Z}_j = ij(S+\bar{\eta}+1+i\Delta)Z_j + \frac{i}{2}j(S+\bar{\eta}-1+i\Delta)(Z_{j+1}+Z_{j-1}) + \frac{\sigma^2 j}{4}[(1-2j)Z_{j-1} - (1+2j)Z_{j+1} - 3jZ_j] + \frac{\sigma^2 j}{8}[(1-j)Z_{j-2} - (1+j)Z_{j+2}], \quad j \geqslant 1, \tag{13}$$

where $Z_0 = 1$. The synaptic current (2) is expressed through the parameters Z_j as

$$S = \frac{JV_{\rm th}}{2\pi}\left[\pi - \theta_{\rm th} - 2\,{\rm Im}\sum_{j=1}^{\infty}\frac{Z_j}{j}((-1)^j - e^{-ij\theta_{\rm th}})\right], \tag{14}$$

where

$$\theta_{\rm th} = 2\arctan(V_{\rm th}). \tag{15}$$

In the absence of noise $\sigma = 0$, the system of Eqs. (13) has an exact solution,

$$Z_j = (Z_1)^j, \tag{16}$$

known as an Ott-Antonsen invariant manifold or OA *Ansatz* [5,6]. This reduces the system (13) to just one differential equation for the first (main) order parameter $Z \equiv Z_1$:

$$\dot{Z} = \frac{i}{2}[(S+\bar{\eta}+i\Delta)(Z+1)^2 - (Z-1)^2]. \tag{17}$$

The synaptic current (14) is expressed through the parameter Z as

$$S = \frac{JV_{\rm th}}{2\pi}\left[\pi - \theta_{\rm th} - 2\arg\left(\frac{1-e^{-i\theta_{\rm th}}Z}{Z+1}\right)\right]. \tag{18}$$

Equations (17) and (18) make up a closed low-dimensional model for the noiseless network of synaptically coupled QIF neurons. This model was analyzed in Ref. [24] using other variables that correspond to the order parameters of the LA *Ansatz*.

In the presence of noise, $\sigma \neq 0$, the system of Eqs. (13) does not satisfy the OA *Ansatz* (16), and we have to deal with an infinite number of the variables $Z_j(t)$, $j = 1,\ldots,\infty$. An approximate solution of this system can be found by truncating it at some $j = M$, i.e., assuming that $Z_j(t) \equiv 0$ for $j > M$. However, the convergence of the solution with increasing M may be slow, and to ensure sufficient accuracy, we may need to solve a large number of equations, say $M \sim 100$. Especially bad convergence occurs in states with high synchrony, where $|Z_1| \approx 1$, since the parameters Z_j decay slowly with j [see Fig. 8(a) in the Appendix].

Recently, Tyulkina *et al.* [31] presented an efficient generalization of the OA *Ansatz* in the case of weak noise, $\sigma \ll 1$. They proposed to rewrite the equations for the Z_j parameters in terms of cumulants. It turned out that such a reformulation of the problem is suitable for the perturbation approach. The authors showed that for small σ, one can be limited by only two-cumulant equations. Below, we use this approach to obtain a low-dimensional model for the ensemble of noisy QIF neurons interacting via synaptic pulses.

C. Cumulant equations

To write down the basic expressions necessary for the low-dimensional reduction of the system (13) and (14), we briefly describe the main ideas of Ref. [31]. According to this reference, order parameters $Z_j = \langle e^{ij\theta}\rangle$ can be treated as moments of the observable $e^{i\theta}$. They are determined via the power series of the moment-generating function:

$$F(k) = \langle \exp(ke^{i\theta})\rangle \equiv \sum_{j=0}^{\infty} Z_j\frac{k^j}{j!}. \tag{19}$$

The circular cumulants κ_j, introduced in [31], are determined from the power series of the cumulant-generating function:

$$\Psi(k) = k\frac{\partial}{\partial k}\ln F(k) \equiv \sum_{j=1}^{\infty}\kappa_j k^j. \tag{20}$$

From Eqs. (19) and (20) one can find the relationship between κ_j and Z_j and thus rewrite Eqs. (13) and (14) in terms of cumulants κ_j. For the first two cumulants, this relationship is as follows:

$$\kappa_1 = Z_1, \quad \kappa_2 = Z_2 - Z_1^2. \tag{21}$$

The benefit of cumulants becomes evident when considering the case of small noise. Without noise, the moments satisfy

the OA *Ansatz* (16), and from Eqs. (19) and (20) we have $F(k) = e^{kZ_1}$ and $\Psi(k) = kZ_1$. It follows that only the first cumulant is nonzero, $\kappa_1 = Z_1$, and all the higher cumulants are zero: $\kappa_j = 0$ for $j > 1$. In the presence of noise, all the cumulants are generally nonzero. However, for small noise, the cumulants with orders larger than 1 are small. In Ref. [31], the dependence of the cumulants on the noise amplitude was estimated as $|\kappa_j| \sim \sigma^{2(j-1)}$. The universality of this scaling law was recently demonstrated in Ref. [33] for various distributions. We verified that this scaling law is also valid for the case of QIF neurons [see Fig. 8(b) in the Appendix]. Given this scaling law, the authors of Ref. [31] proposed a simple approximation that takes into account only the first two cumulants κ_1 and κ_2 and neglecting all higher cumulants. The accuracy of such an approximation is $O(\sigma^4)$. With the given accuracy, the moments Z_j can be expressed through these two cumulants as

$$Z_j = Z_1^j + \kappa_2 Z_1^{j-2}[j(j-1)]/2. \tag{22}$$

Taking into account the above expressions, we obtained the following two-cumulant approximation for the system (13):

$$\dot{Z} = \frac{i}{2}[(S + \bar{\eta} + i\Delta)(Z+1)^2 - (Z-1)^2] - \frac{\sigma^2}{4}(Z+1)^3 + \frac{\kappa}{2}\left[i(S + \bar{\eta} + i\Delta - 1) - \frac{3}{2}\sigma^2(Z+1)\right], \tag{23a}$$

$$\dot{\kappa} = \kappa\{2i[(Z+1)(S + \bar{\eta} + i\Delta) - Z + 1] - 3\sigma^2(Z+1)^2\} - \frac{\sigma^2}{4}(Z+1)^4. \tag{23b}$$

Here, for simplicity, the notations $Z \equiv \kappa_1 = Z_1$ and $\kappa \equiv \kappa_2 = Z_2 - Z_1^2$ for the first two cumulants are used. In the two-cumulant approximation, the expression (14) for a synaptic current is reduced to

$$S = \frac{JV_{\text{th}}}{2\pi}\left\{\pi - \theta_{\text{th}} - 2\arg\left(\frac{1 - e^{-i\theta_{\text{th}}}Z}{Z+1}\right) - \text{Im}\left[\kappa\left(\frac{1}{(1+Z)^2} - \frac{1}{(e^{i\theta_{\text{th}}} - Z)^2}\right)\right]\right\}. \tag{24}$$

Equations (23) and (24) represent a low-dimensional model for describing the evolution of a noisy QIF neural network. For $\sigma = 0$ and $\kappa = 0$, this model coincides with the noiseless model defined by Eqs. (17) and (18). In the next section, we use the reduced model of Eqs. (23) and (24) to analyze the effect of noise on network dynamics. We also compare the solutions of this model with the solutions of a large system of Eqs. (13) and (14), as well as with the results of numerical simulation of the microscopic model (4) for a finite number of neurons.

III. NUMERICAL ANALYSIS

We begin our analysis from the case of an excitable network, when all free neurons in the network are excitable. For the Lorentz distribution (11) of the parameter η, the absence of spiking neurons requires that the distribution parameters be $\Delta = 0$ and $\bar{\eta} < 0$. This corresponds to a network of identical excitable neurons. We consider this problem in Sec. III A, and the effect of neural heterogeneity ($\Delta \neq 0$) is discussed in Sec. III B. Numerical analysis shows that macroscopic oscillations do not occur in a network of excitable neurons when the coupling is inhibitory ($J < 0$). Therefore, below we present the bifurcation diagrams only for the excitatory ($J > 0$) coupling.

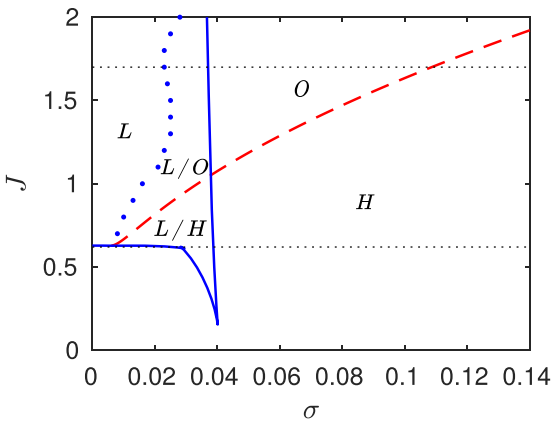

FIG. 1. Bifurcation diagram of the two-cumulant approximation [Eqs. (23) and (24)] in the (σ, J) plane for fixed $V_{\text{th}} = 5$ and $\bar{\eta} = -0.01$. The solid blue curve represents the saddle-node bifurcation of fixed points, the dashed red curve shows the supercritical Hopf bifurcation, and the dotted blue curve indicates the homoclinic bifurcation or the end of the quasiperiodic oscillation. The regions marked with different letters correspond to different dynamic modes: L and H, stable equilibrium regimes with low and high synaptic activity, respectively; O, the limit-cycle oscillations; L/H, bistable mode with low and high constant values of synaptic current; L/O denotes a bistable mode with low constant synaptic activity and limit-cycle oscillations. Two horizontal dotted lines ($J = 0.62$ and 1.7) show cross sections of the bifurcation diagram, which are analyzed in Figs. 2 and 3 in more detail.

A. Network of identical excitable neurons

The reduced model of Eqs. (23) and (24) is convenient for bifurcation analysis, because it contains only two complex dynamic variables: Z and κ. Generally, the behavior of the model depends on five parameters: Δ, $\bar{\eta}$, J, σ, and V_{th}. Here we consider the case of identical neurons, so $\Delta = 0$. In the bifurcation analysis, one of the remaining four parameters can be fixed without loss of generality. This was shown in Ref. [23] by rescaling the parameters of the Fokker-Planck equation for the membrane potential. Here we fix the value of the parameter $\bar{\eta}$ and analyze the behavior of the system depending on the parameters J, σ, and V_{th}.

Figure 1 shows the bifurcation diagram of Eqs. (23) and (24) in the (σ, J) plane for fixed $V_{\text{th}} = 5$ and $\bar{\eta} = -0.01$. The diagram was built using the MATCONT package [52]. The plane is divided into five areas by three bifurcation curves: the solid blue curve represents the saddle-node bifurcation of fixed points, the dashed red curve shows the supercritical Hopf bifurcation, and the dotted blue curve indicates the homoclinic bifurcation or the end of the quasiperiodic oscillation. Note that quasiperiodic solutions do not appear in a more accurate model described by a large system of Eqs. (13) and (14); they are artifacts of the two-cumulant approximation associated with truncation of the cumulant equations. Five

regions marked with different letters correspond to different dynamic modes: L denotes a stable equilibrium mode with low synaptic activity (low constant values of synaptic current S) in which almost all neurons are quenched; H is another stable equilibrium mode with high synaptic activity (high constant values of synaptic current), where almost all neurons fire, but incoherently, therefore the mean field is constant; O denotes the area where a large part of the neurons fire coherently and produce macroscopic periodic oscillations; L/H denotes a bistable region with low and high constant synaptic current values; and finally, L/O denotes a bistable mode with low constant synaptic activity and macroscopic oscillations.

To verify the accuracy of the above bifurcation diagram, we compared the solutions of the two-cumulant Eqs. (23) and (24) with "exact" results obtained from a large ($M = 150$) system of Eqs. (13) and (14), as well as the results of numerical simulation of a stochastic microscopic model (4), consisting of $N = 2000$ theta neurons. The microscopic model was integrated by the Euler-Heun method, with a time step $\Delta t = 0.001$. The two other models were integrated by the standard Runge-Kutta 4/5 scheme. Below we present the results for two different fixed values of the coupling strength $J = 0.62$ and 1.7, which correspond to the two cross sections of the bifurcation diagram shown in the Fig. 1 with dotted horizontal lines.

For fixed $J = 0.62$ (bottom dotted line in Fig. 1), the two-cumulant model predicts one or two stable equilibrium states (fixed points) depending on the noise amplitude; the number of stable equilibrium states changes via saddle-node bifurcations of fixed points, which occur at the intersection of the blue curve with the dashed line. Figure 2 shows the dependence of the synaptic current S on the noise amplitude σ for fixed $J = 0.62$ obtained by the three different methods mentioned above: the green squares correspond to the two-cumulant approximation, the blue circles show the "exact" results obtained from Eqs. (13), and the red asterisks represent the results of a stochastic microscopic model (4). In the latter case, the synaptic current is a stochastic variable, and here we show its time average value. To reveal the bistability, the amplitude σ of the noise was changed in the forward (upper panel) and reverse (lower panel) directions. We see a hysteresis in the dependence of S on σ for all three models. Thus, the low-dimensional model (23) correctly predicts the existence of the L/H bistability, although the exact values of the noise amplitude, at which the synaptic current undergoes jumps from small to large values and vice versa, differ for different models. Note that synaptic current values outside the hysteresis are in good agreement for all three models. In addition, we remark that although true bistability in noisy systems can take place only in the thermodynamic limit, numerical simulation of a finite-size microscopic model shows extremely long residence times close to each stable equilibrium (see the caption of Fig. 2). Similar effects were described in Ref. [23].

For a larger value of the coupling strength $J = 1.7$, the influence of noise on the asymptotic dynamics of the network becomes more interesting (see the upper dotted line in Fig. 1). Here, along with stable equilibrium states, the limit-cycle oscillations occur. To demonstrate such noise-induced oscillations, in Fig. 3 we plot the dependence of the variance $\mathrm{Var}(S)$ of the synaptic current on the noise amplitude for fixed $J = 1.7$. Zero or small values of the variance correspond to nonoscillating states, while large values of the variance indicate macroscopic oscillations of the network. Here, as in

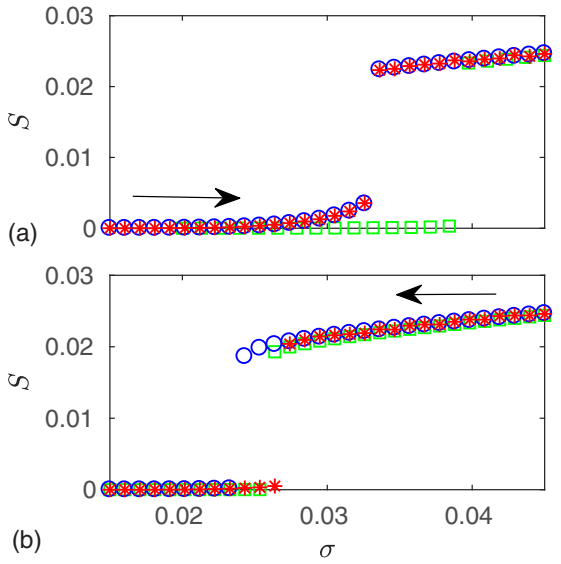

FIG. 2. The dependence of the synaptic current S on the noise amplitude σ for fixed $J = 0.62$: (a) forward continuation and (b) backward continuation. The continuations were performed with a step size $\Delta\sigma = 10^{-3}$. At each step, the system was idly integrated for a period $T = 1500$ to eliminate transient. The values of the parameters are $V_{\mathrm{th}} = 5$ and $\bar{\eta} = -0.01$. The green squares show the solution of the two-cumulant Eqs. (23) and (24), the blue circles show the "exact" results obtained from a large ($M = 150$) system of Eqs. (13) and (14), and the red asterisks show the results of numerical simulation of a stochastic microscopic model (4), consisting of $N = 2000$ theta neurons.

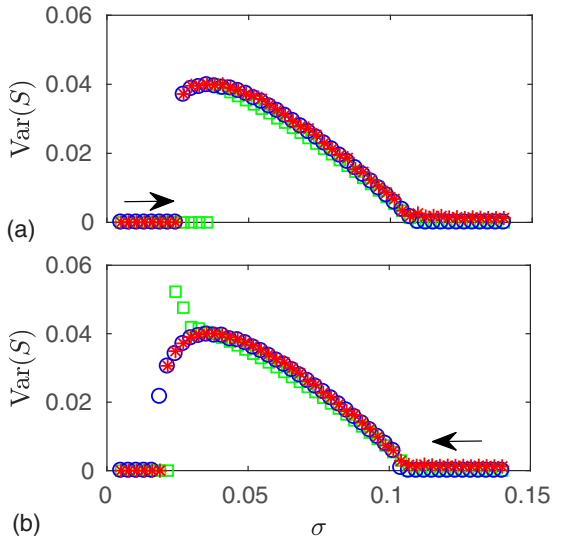

FIG. 3. The forward (a) and backward (b) continuations of the variance $\mathrm{Var}(S)$ of the synaptic current for the coupling strength $J = 1.7$. Other parameters and markings are the same as in Fig. 2.

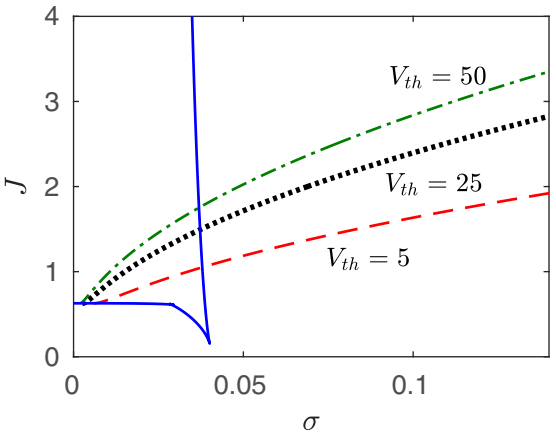

FIG. 4. The influence of the width of synaptic pulses determined by the threshold potential V_{th} on the Hopf and saddle-node bifurcations. The bifurcation curves are presented for three different values of V_{th}: 5, 25, and 50. The corresponding Hopf bifurcation curves are shown by dashed red, dotted black, and dashed-dotted green curves. The saddle-node bifurcation curves (solid blue curve) practically coincide for all given values of V_{th}.

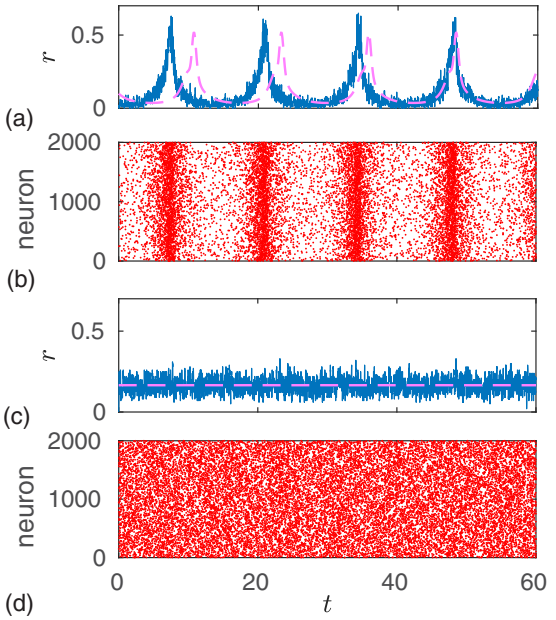

FIG. 5. Spiking rate (a) and raster plot (b) for the oscillating mode at $\sigma = 0.05$, $J = 1.7$, and $V_{\text{th}} = 5$. The solid blue and dashed pink curves show the results obtained from the stochastic microscopic model (4) consisting of $N = 2000$ neurons and two-cumulant approximation [Eqs. (23), (24), and (25)], respectively. Dots in the raster plot correspond to firing events of individual neurons. Parts (c) and (d) show the same results as in (a) and (b), respectively, but for the stable equilibrium mode with high synaptic activity at the parameters $\sigma = 0.12$, $J = 1.7$, and $V_{\text{th}} = 5$. Spiking rate of the microscopic system is smoothed by using a moving average with a time window of size $\delta t = 10^{-2}$.

Fig. 2, we present forward and backward continuations of this characteristic for the above three different models using the same symbolic notations. Again, we see that the two-cumulant Eqs. (23) and (24) describe well the asymptotic behavior of the network in the entire range of σ, with the exception of a narrow hysteresis region, where L/O bistability occurs. We tried to improve the results in this region by testing various methods of truncating the cumulant equations. Along with the closure $\kappa_3 = 0$ used here, we checked two other closures $\kappa_3 = (3/2)\kappa_2^2/Z_1$ and $(3/2)\kappa_2^2 Z_1^*$ proposed in Ref. [32]. In both cases, no tangible benefit was obtained.

Figure 3 shows that noise acts in two antagonistic ways: while sufficient noise intensity can excite quenched neurons, causing a synchronized firing, large-amplitude noise deteriorates the synchronization properties of the network. As a result, coherent firing is observed only for an intermediate noise level, similar to the classical coherence resonance [35]. Unlike classical coherence resonance, which deals with one noise driven excitable element, here we are dealing with a network of interacting excitable neurons. In our network, noise-excited neurons synchronize due to synaptic interaction and produce coherent macroscopic oscillations. The fact that coupling can enhance noise-induced coherence in excitable systems was reported for an array of diffusely coupled FitzHugh-Nagumo neurons in Refs. [43,44].

We also investigated the effect of the width of synaptic pulses, determined by the threshold potential V_{th}, on the Hopf bifurcation. The results are presented in Fig. 4. Here, Hopf curves are plotted in the (σ, J) plane for three different values of the threshold potential V_{th}. We see that for a fixed noise intensity, an increase in V_{th} (a decrease in the width of synaptic pulses) shifts the threshold of macroscopic oscillations toward higher values of the coupling strength J. For $V_{\text{th}} \to \infty$, the threshold of the coupling strength tends to infinity, so that macroscopic oscillations become impossible for any finite J and σ. Thus, macroscopic oscillations in the noisy network of QIF neurons, as well as in the deterministic network considered in Ref. [23], cannot occur in the case of interaction via instantaneous pulses. Interestingly, a change in V_{th} has almost no effect on the saddle-node bifurcation. The saddle-node bifurcation curves, shown in Fig. 4 for different values of V_{th}, are indistinguishable.

In experimental neuroscience, the dynamic properties of neural populations are usually analyzed by measuring the firing rate. In Fig. 5 we present the dynamics of this characteristic estimated from the microscopic model (4), and we compare it with that obtained from the two-cumulant approximation (23). We demonstrate this for two different dynamic modes, namely the mode of macroscopic oscillations [Figs. 5(a) and 5(b)] and the mode of stable equilibrium with high synaptic activity [Figs. 5(a) and 5(b)]. For the microscopic model, the firing rate is just the number of neurons that cross the phase $\theta = \pi$ in one integration step size Δt divided by Δt. In Figs. 5(a) and 5(c) this is shown by solid blue curves. In the thermodynamic limit, the firing rate $r(t)$ is defined as a probability flux at $\theta = \pi$: $r(t) = 2\rho(\pi|\bar{\eta} + i\Delta, t)$. For the two-cumulant approximation, this gives the following expression:

$$r(t) = \frac{1 - |Z|^2}{\pi|1 + Z|^2} + \text{Re}\left[\frac{2\kappa}{\pi(1 + Z)^3}\right]. \tag{25}$$

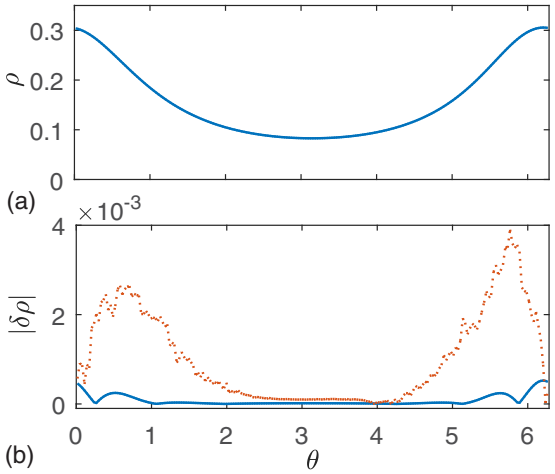

FIG. 6. (a) "Exact" PDF of a stable equilibrium mode with high synaptic activity estimated from a large ($M = 150$) system of Eqs. (13) and (14). The parameter values are the same as in Figs. 5(c) and 5(d). (b) The absolute value of the difference between "exact" PDF and PDF, estimated from the two-cumulant approximation (solid blue curve), as well as "exact" PDF and PDF, estimated from the stochastic microscopic model (4), consisting of $N = 2000$ neurons (red dotted curve).

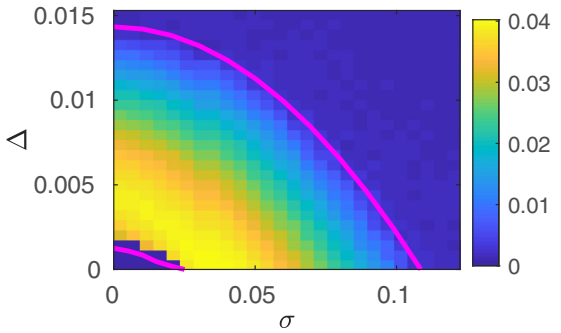

FIG. 7. A plot of the variance Var(S) of the synaptic current in the (σ, Δ) plane, estimated from the numerical simulation of the stochastic microscopic model (4). The solid pink curves show the boundaries of limit-cycle oscillations, obtained from the two-cumulant approximation (23) and (24). Parameters: $J = 1.7$, $\bar{\eta} = -0.01$, $V_{\text{th}} = 5$, and $N = 2000$.

This expression is obtained using the relation defined by Eq. (22). Since the accuracy of Eq. (22) is $O(\sigma^4)$, it follows that the accuracy of the spiking rate Eq. (25) is also $O(\sigma^4)$. Note that Goldobin and Dolmatova [33] have recently shown that the cumulant-generating function, which consists of only two nonzero cumulants, leads to a divergence of the firing rate. However, in the presence of a small parameter and the hierarchy of cumulants, the spiking rate can be estimated with any given accuracy. The estimation of the spiking rate with the accuracy $O(\sigma^4)$ presented in Ref. [33] coincides with our Eq. (25). In Figs. 5(a) and 5(c), the spiking rate is shown by dotted pink curves. For the oscillatory mode [Fig. 5(a)], it does not exactly match the firing rate estimated from the microscopic model, but it has a similar amplitude and frequency. For equilibrium mode [Fig. 5(c)], the results of the two-cumulant and microscopic models are in good agreement: the two-cumulant approximation gives the mean value of the fluctuating firing rate of the microscopic model. In the latter case, fluctuations occur due to the finite size of the network, while in the first case there are no fluctuations because of the infinite size of the network. To visualize the behavior of the system at the microscopic level, in Figs. 5(b) and 5(d) we present the spike raster plots for the oscillating and equilibrium modes, respectively. In the first case, the raster plot shows highly correlated spikes, while in the second case the spikes of the neurons are not correlated.

Finally, in Fig. 6 we plot a stationary PDF $\rho(\theta|\bar{\eta}, t) \equiv \rho(\theta)$ corresponding to a stable equilibrium mode with high synaptic activity at the same values of the parameter used in Figs. 5(c) and 5(d). Figure 6(a) shows the "exact" PDF obtained from a large ($M = 150$) system of Eqs. (13) and (14). To estimate the accuracy of the two-cumulant approximation, in Fig. 6(b) we show (solid blue curve) the absolute value of the difference $|\delta\rho(\theta)|$ between the "exact" PDF and the PDF estimated from the two-cumulant approximation. The maximal error of the two-cumulant approximation is $\max[|\delta\rho(\theta)|] \approx 5 \times 10^{-4}$. For a given noise amplitude $\sigma = 0.12$, this result confirms the fact that the accuracy of the two-cumulant approximation is $O(\sigma^4)$ [31]. In this figure, we also show (dotted red curve) the absolute value of the difference between the "exact" PDF and the PDF, estimated from a stochastic microscopic model (4) consisting of $N = 2000$ neurons. Here, the maximum deviation between the PDFs is $\approx 4 \times 10^{-3}$. This deviation is mainly due to the fact that the "exact" PDF corresponds to a network of infinite size, and the PDF, estimated by Eqs. (4), corresponds to a network of finite size.

B. The effect of neural heterogeneity

To test the robustness of macroscopic oscillations caused by noise, we investigated an influence of neural heterogeneity on the occurrence of such oscillations. In our model, the heterogeneity of neurons is determined by the width Δ of the Lorentzian distribution (11) of the parameter η. In Fig. 7 we present a color plot of the variance Var(S) of the synaptic current in the (σ, Δ) parameter plane, estimated from the stochastic microscopic model (4), and we compare it with the bifurcation diagram, obtained from the two-cumulant approximation. The two-cumulant Eqs. (23) and (24) predict the limit-cycle oscillations in the region lying between two solid pink curves. This prediction is in good agreement with the simulation of the stochastic microscopic model: small values of the parameter Var(S) correspond to a stable equilibrium of the network, while large values indicate macroscopic oscillations. We see that noise-induced oscillations exist when $\Delta > 0$, which means that they are robust with respect to the heterogeneity of neurons. Moreover, heterogeneity is a favorable factor for the occurrence of macroscopic oscillations, and its influence on this phenomenon is similar to the effect of noise. This can be seen from the shape of the (σ, Δ) diagram; its topology remains unchanged after a symmetric transformation along the diagonal.

IV. DISCUSSION

In this paper, we analyzed the dynamics of a large network of globally coupled quadratic integrate-and-fire neurons subjected to independent local noise. The interaction between neurons is determined by synaptic pulses of a finite width. The quadratic integrate-and-fire neuron is the canonical model for the class I neurons in which spiking instability occurs through a saddle-node bifurcation on an invariant curve. Using a standard change of variables, we transformed a network of quadratic integrate-and-fire neurons into an equivalent network of theta neurons, and we considered this network in the limit of infinite size. This allowed us to apply the newly developed perturbation method [31] to reduce the corresponding Fokker-Planck equation to a low-dimensional dynamical system determined by only two circular cumulants. The two-cumulant approximation is a natural extension of the Ott-Antonsen *Ansatz* [5], applied to purely deterministic systems, for the case of dynamical systems with small noise.

We used the advantage of the reduced two-cumulant equations in order to perform a bifurcation analysis of the system depending on various network parameters. For a network consisting of identical excitable neurons, we found three different modes: two of them are stable equilibrium states with low and high synaptic activity, and the third is a mode of limit-cycle oscillations. We also detected two regions of bistability with a mixture of the above two states of equilibrium or a state of equilibrium and oscillations of the limit cycle.

The most interesting mode of the network is the limit-cycle oscillations. Here, the initially quenched neurons are excited by noise, and their spikes are synchronized due to the interaction, so that an oscillating macroscopic field is formed. Such oscillations occur for a sufficiently high coupling strength and for intermediate noise amplitudes. When the noise amplitude decreases or increases, the system goes out of the oscillation mode and enters a stable equilibrium mode with low or high synaptic activity, respectively. We also investigated the effect of neural heterogeneity on the excitation of macroscopic oscillations. Our studies have shown that heterogeneity is a favorable factor for the occurrence of macroscopic oscillations, and its influence on this phenomenon is similar to the effect of noise. Note that global oscillations caused by heterogeneous coupling were reported in an inhibitory network of spiking QIF neurons in Ref. [28].

We verified the accuracy of the two-cumulant approximation, comparing it with the "exact" solution of the Fokker-Planck equation. The latter was obtained by expanding the probability density function in a truncated Fourier series and solving a large system of differential equations for the Fourier amplitudes. This comparison showed that the two-cumulant approximation gives good results almost everywhere, except for narrow regions of bistability. The two-cumulant equations correctly predict the existence of bistabilities, although the predicted boundaries of the bistabilities differ from the exact boundaries. In general, we can conclude that the two-cumulant approximation is a good low-dimensional model for describing the dynamics of a noisy infinite-size network of synaptically coupled QIF neurons. We also showed that this model is well suited for predicting the dynamics of finite-size networks. This was demonstrated by comparing its solutions with the results of direct numerical simulation of a microscopic model of a stochastic network consisting of 2000 synaptically coupled neurons.

This paper extends the research of Refs. [19–29], devoted to a low-dimensional description of the dynamics of noiseless globally coupled QIF or theta neuron networks, to the case of noisy networks. Such model networks are universal in the sense that they describe the dynamics of coupled canonical class I neurons, which are modeled by a normal-form equation that is universal near the spiking threshold. The low-dimensional models derived from the microscopic spiking neurodynamics can be considered as an alternative to the phenomenological neural mass models that are used to simulate the coarse-grained activity of large populations of neurons [50]. The two-cumulant model of the noisy QIF neural network can be useful for testing new neural stimulation protocols needed for medical applications.

ACKNOWLEDGMENTS

The authors are thankful to Denis Goldobin for reading our manuscript and useful comments. This work was supported by Grant No. S-MIP-17-55 of the Research Council of Lithuania.

APPENDIX: HIERARCHY OF CUMULANTS IN QIF NEURON NETWORK

In Fig. 8, we show the dependence of the order parameters $|Z_j|$ and the cumulants $|\kappa_j|$ on the index j for different values of the noise amplitude σ^2. The order parameters were estimated using the truncated system of Eqs. (13) and (14) with $M = 300$. We see that the cumulants decay faster than the order parameters. What is more important, the linear dependence on the semilog graph in Fig. 8(b) indicates that the cumulants' hierarchy satisfies the scaling law $\kappa_j \propto \sigma^{2(j-1)}$.

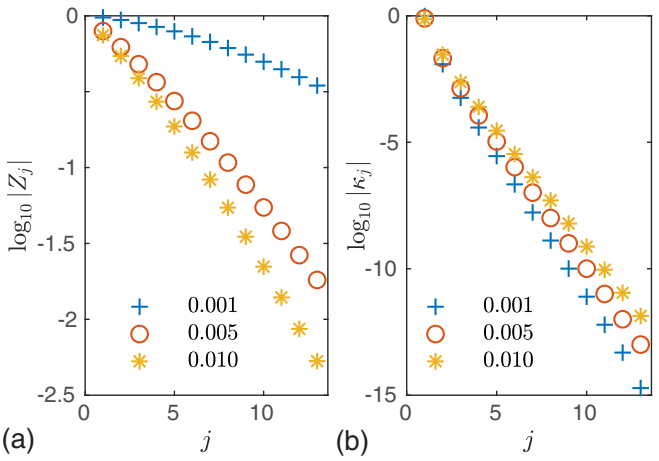

FIG. 8. (a) Order parameters $|Z_j|$ and (b) circular cumulants $|\kappa_j|$ are plotted for $\bar{\eta} = -0.01$, $V_{\text{th}} = 5$, $\Delta = 0$, and different values of the noise amplitude: $\sigma^2 = 0.01$ (stars), $\sigma^2 = 0.005$ (circles), and $\sigma^2 = 0.001$ (crosses).

[1] Y. Kuramoto, *Chemical Oscillations, Waves and Turbulence* (Springer-Verlag, New York, 1984), Vol. 39.

[2] A. Pikovsky, M. Rosenblum, and J. Kurths, *Synchronization: A Universal Concept in Nonlinear Sciences* (Cambridge University Press, Cambridge, 2001).

[3] A. Balanov, N. Janson, D. Postnov, and O. Sosnovtseva, *Synchronization: From Simple to Complex* (Springer-Verlag, Berlin, 2009).

[4] Y. Kuramoto, in *International Symposium on Mathematical Problems in Theoretical Physics*, edited by H. Araki, Lecture Notes in Physics Vol. 39 (Springer-Verlag, New York, 1975), Vol. 39.

[5] E. Ott and T. M. Antonsen, Chaos **18**, 037113 (2008).

[6] E. Ott and T. M. Antonsen, Chaos **19**, 023117 (2009).

[7] E. A. Martens, E. Barreto, S. H. Strogatz, E. Ott, P. So, and T. M. Antonsen, Phys. Rev. E **79**, 026204 (2009).

[8] E. Ott, B. R. Hunt, and T. M. Antonsen, Chaos **21**, 025112 (2011).

[9] A. Pikovsky and M. Rosenblum, Physica D **240**, 872 (2011).

[10] H. Hong and S. H. Strogatz, Phys. Rev. Lett. **106**, 054102 (2011).

[11] M. Wolfrum, S. V. Gurevich, and O. E. Omel'chenko, Nonlinearity **29**, 257 (2016).

[12] A. Pikovsky and M. Rosenblum, Chaos **25**, 097616 (2015).

[13] A. Schnitzler and J. Gross, Nat. Rev. Neurosci. **6**, 285 (2005).

[14] W. W. Alberts, E. W. Wright, and B. Feinstein, Nature (London) **221**, 670 (1969).

[15] F. A. Lenz, H. C. Kwan, R. L. Martin, R. R. Tasker, J. O. Dostrovsky, and Y. E. Lenz, Brain **117**, 531 (1994).

[16] J. A. Goldberg, U. Rokni, T. Boraud, E. Vaadia, and H. Bergman, J. Neurosci. **24**, 6003 (2004).

[17] A. Nini, A. Feingold, H. Slovin, and H. Bergman, J. Neurophysiol. **74**, 1800 (1995).

[18] G. Bard Ermentrout and D. H. Terman, *Mathematical Foundations of Neuroscience* (Springer, New York, 2010).

[19] T. B. Luke, E. Barreto, and P. So, Neural Comput. **25**, 3207 (2013).

[20] P. So, T. B. Luke, and E. Barreto, Physica D **267**, 16 (2014).

[21] T. B. Luke, E. Barreto, and P. So, Frontiers Comput. Neurosci. **8**, 1 (2014).

[22] C. R. Laing, Phys. Rev. E **90**, 010901(R) (2014).

[23] E. Montbrió, D. Pazó, and A. Roxin, Phys. Rev. X **5**, 021028 (2015).

[24] I. Ratas and K. Pyragas, Phys. Rev. E **94**, 032215 (2016).

[25] D. Pazó and E. Montbrió, Phys. Rev. Lett. **116**, 238101 (2016).

[26] I. Ratas and K. Pyragas, Phys. Rev. E **98**, 052224 (2018).

[27] F. Devalle, A. Roxin, and E. Montbrió, PLOS Comput. Biol. **13**, e1005881 (2017).

[28] M. di Volo and A. Torcini, Phys. Rev. Lett. **121**, 128301 (2018).

[29] I. Ratas and K. Pyragas, Phys. Rev. E **96**, 042212 (2017).

[30] A. Longtin, Effects of noise on nonlinear dynamics, in *Nonlinear Dynamics in Physiology and Medicine*, edited by A. Beuter, L. Glass, M. C. Mackey, and M. S. Titcombe (Springer, New York, 2003), pp. 149–189.

[31] I. V. Tyulkina, D. S. Goldobin, L. S. Klimenko, and A. Pikovsky, Phys. Rev. Lett. **120**, 264101 (2018).

[32] D. S. Goldobin, I. V. Tyulkina, L. S. Klimenko, and A. Pikovsky, Chaos **28**, 101101 (2018).

[33] D. S. Goldobin and A. V. Dolmatova, arXiv:1908.00230.

[34] V. Anishchenko, V. Astakhov, A. Neiman, T. Vadivasova, and L. Schimansky-Geier, *Nonlinear Dynamics of Chaotic and Stochastic Systems* (Springer-Verlag, Berlin, 2007).

[35] A. S. Pikovsky and J. Kurths, Phys. Rev. Lett. **78**, 775 (1997).

[36] S. Shinomoto and Y. Kuramoto, Prog. Theor. Phys. **75**, 1105 (1986).

[37] C. Kurrer and K. Schulten, Phys. Rev. E **51**, 6213 (1995).

[38] S. H. Park and S. Kim, Phys. Rev. E **53**, 3425 (1996).

[39] C. J. Tessone, A. Scirè, R. Toral, and P. Colet, Phys. Rev. E **75**, 016203 (2007).

[40] B. Sonnenschein, M. Zaks, A. Neiman, and L. Schimansky-Geier, Eur. Phys. J. Spec. Top. **222**, 2517 (2013).

[41] J. Pham, K. Pakdaman, and J.-F. Vibert, Phys. Rev. E **58**, 3610 (1998).

[42] J. Touboul, G. Hermann, and O. Faugeras, SIAM J. Appl. Dyn. Syst. **11**, 49 (2012).

[43] B. Hu and C. Zhou, Phys. Rev. E **61**, 1001(R) (2000).

[44] C. Zhou, J. Kurths, and B. Hu, Phys. Rev. Lett. **87**, 098101 (2001).

[45] M. A. Zaks, A. B. Neiman, S. Feistel, and L. Schimansky-Geier, Phys. Rev. E **68**, 066206 (2003).

[46] J. A. Acebrón, A. R. Bulsara, and W.-J. Rappel, Phys. Rev. E **69**, 026202 (2004).

[47] M. A. Zaks, X. Sailer, L. Schimansky-Geier, and A. B. Neiman, Chaos **15**, 026117 (2005).

[48] M. Masoliver, N. Malik, E. Schöll, and A. Zakharova, Chaos **27**, 101102 (2017).

[49] B. Lindner, J. Garcia-Ojalvo, A. Neiman, and L. Schimansky-Geier, Phys. Rep. **392**, 321 (2004).

[50] S. Coombes and A. Byrne, Next generation neural mass models, *Nonlinear Dynamics in Computational Neuroscience* (Springer, Cham, 2019), pp. 1–16.

[51] N. G. van Kampen, J. Stat. Phys. **24**, 175 (1981).

[52] A. Dhooge, W. Govaerts, and Y. A. Kuznetsov, ACM Trans. Math. Software **29**, 141 (2003).